

IMECE2007-42751

**EQUILIBRIUM STRUCTURE OF A 1-DOF ELECTROSTATIC
MEMS MODEL WITH PARASITICS**

D. H. S. Maithripala

Faculty of Engineering
University of Ruhuna
Galle, Sri Lanka

E-mail: smaithri@mme.ruh.ac.lk

B. D. Kawade

Oceaneering International, Inc.
Houston, TX

E-mail: BKawade@oceaneering.com

I. P. M. Wickramasinghe

Dept. of Mechanical Engineering
Texas Tech University
Lubbock, TX 79409

E-mail: m.wickramasinghe@ttu.edu

J. M. Berg*

Dept. of Mechanical Engineering
Texas Tech University
Lubbock, TX 79409

E-mail: jordan.berg@ttu.edu

W. P. Dayawansa

Deceased; formerly
Dept. of Mathematics and Statistics
Texas Tech University
Lubbock, TX 79409

ABSTRACT

Feedback control of electrostatic microelectromechanical systems (MEMS) is significantly complicated by the presence of parasitic surfaces. This note considers the stabilization of a one-degree-of-freedom (1-DOF) piston actuator with capacitively-coupled parasitics. Previous work by the authors has shown how, in the absence of parasitics, any feasible equilibrium point of this system may be made globally asymptotically stable using passivity-based control. However if parasitics are present this nominal closed-loop system may be destabilized by capacitive coupling, through a phenomenon called charge pull-in. This note shows how the nominal controller formulation may be modified to eliminate multiple equilibria. If the movable electrode is completely screened from the parasitic electrode by the control electrode, the unique equilibrium is globally asymptotically stable. Otherwise, though the desired equilibrium is still unique, its region of attraction may be finite and the equilibrium may lose stability through a Hopf bifurcation.

INTRODUCTION

Electrostatic actuation of microelectromechanical systems (MEMS) makes use of the attractive coulomb forces that develop between capacitively-coupled conductors differing in voltage. Electrostatic actuation is nonlinear, making open-loop control over a large operating range difficult. Furthermore, the non-linearity gives rise to a saddle-node bifurcation known as *voltage pull-in* that necessitates operational limitations. Eliminating this effect would allow for enhanced functionality in a number of applications by increasing the operational range of the movable electrode, reducing the need for motion limiters and anti-stiction measures, and preventing disturbances from causing the movable electrode to depart from its stable operating region.

A number of controls approaches have been presented in the literature to address pull-in. In the context of the current paper the most relevant are those that—implicitly or explicitly—make use of the substantial improvements in stability associated with control of electrode charge versus control of electrode voltage. Some notable examples include [10, 14, 16]. However, an additional challenge is to implement these controllers in the presence of dynamics arising from resistive and capacitive coupling both

*To whom correspondence should be addressed.

between device components, and between these components and the surroundings. These interactions are commonly referred to as *parasitics*. It is known that the effects of parasitic capacitance can cause loss of stability of charge-controlled electrostatic MEMS through a saddle-node bifurcation known as *charge pull-in* [4, 5, 12, 14]. Explicit compensation of parasitic effects is only now beginning to attract attention from the controls community, for example [17].

In [2, 7–9] we present a series of results on passivity-based global and semi-global stabilization of electrostatically actuated MEMS. The one-degree-of-freedom case is considered in [7]. The system input and output are the control voltage applied to the fixed electrode and the charge on the movable electrode, respectively. Two controllers are derived that eliminate the pull-in bifurcation and stabilize any point in the capacitive gap. These are the only points for which a feasible equilibrium exists. One controller, based on the energy-shaping version of passivity [13], results in a charge feedback controller. The other, based on feedback passivation techniques [3], requires an additional velocity feedback term. Unlike the energy-shaping controller, the feedback-passivation controller may be used to inject damping into the mechanical subsystem, improving transient performance. The generalized model and controller presented in [8] extends the 1-DOF results to a broad class of electrostatically forced mechanical systems, including a variety of interesting MEMS devices. That extension requires measurement of the voltage and charge associated with all electrodes, including parasitic surfaces. Typically this is not feasible. When these measurements are not available the controllers of [7, 8] may fail to stabilize equilibrium points low in the gap, with loss of stability due to charge pull-in. The main object of the present note is to examine whether the global 1-DOF result of [7] may be recovered in the presence of parasitics without requiring charge or voltage measurements on the parasitic electrodes. The analysis presented here considers only stabilization and not improved transient behavior. The energy-shaping controller and the feedback-passivation controller are equivalent with respect to the location and stability of closed-loop equilibrium points. However so far only the behavior of the energy-shaping controller has been thoroughly studied. The feedback-passivation controller may provide a larger domain of attraction, and may influence the loss of stability through dynamic mechanisms such as Hopf bifurcation. This question is a topic of current research, and further discussion is beyond the scope of the present note.

The model considered is the standard 1-DOF model used in [7]—a grounded movable electrode suspended by a spring and damper above a fixed control electrode—with an additional fixed parasitic electrode added below the control electrode (see Fig. 1). As in [1, 7, 8], the voltage across the movable and fixed electrode is assumed to be measured, along with either the charge on the fixed electrode or the mutual capacitance between the movable and fixed electrodes. In the present note the parasitic electrode is

connected to ground through a resistor. Therefore both the parasitic voltage and the charge can vary dynamically. At equilibrium however the parasitic voltage will be zero. This condition may be relaxed by including a voltage source in series [2], but such an extension is beyond the scope of the present note. Physically the parasitic surface might represent the wafer substrate upon which the MEMS device is fabricated.

It is shown that feedback control using the *total charge* on the movable and parasitic electrodes as system output can prevent charge pull-in, and provide global asymptotic stability of the desired equilibrium. If the control electrode is bigger than either the movable electrode or the parasitic electrode then, neglecting fringing, the parasitic electrode is completely screened from the movable electrode. In this case the total charge feedback law can be implemented using the specified measurements. Otherwise the equilibrium is only locally asymptotically stable, and in fact the equilibrium may itself lose stability through a Hopf bifurcation. Furthermore, the feedback law can not be implemented using the specified measurements and will have to be approximated. This approximation does not affect the location of the equilibrium, but it may further reduce the region of attraction. These effects become more pronounced as the parasitic surface becomes larger with respect to the control surface, or as the parasitic surface moves closer to the control surface.

This note is organized as follows: First we present a 1-DOF model of an electrostatic MEMS with a parasitic capacitance. We then revisit the nominal energy-shaping controller derived in [7, 8] and show how parasitics may cause charge pull-in, which we interpret in terms of bifurcation of the system zero dynamics. We next demonstrate the use of total charge feedback to eliminate charge pull-in and recover global asymptotic stability, and examines how measured quantities may be used to implement this feedback. The controller is demonstrated using Matlab and ANSYS simulations. Finally, we summarize the result and discuss possible extensions.

1-DOF MODEL WITH PARASITIC CAPACITANCE

We consider a MEMS device modeled by three parallel plates. On top is the movable electrode, suspended by spring and damping elements and constrained to translate in the vertical direction, in the middle is a fixed plate that we refer to as the drive or control electrode, and at bottom is a fixed parasitic electrode. The plates have area A_0 , A_c , and A_p , respectively, and are assumed to be centered on a common axis. The zero voltage gap between the moving and drive electrode is d and the distance between the parasitic and drive electrode is δ . Resistive cross-coupling is neglected here, and the movable electrode is assumed to be grounded, that is, connected to ground through a zero voltage bias, with negligible series resistance. Figure 1 shows a schematic of the model. The configuration of the parasitic electrode is motivated by MEMS designs in which a parallel-plate

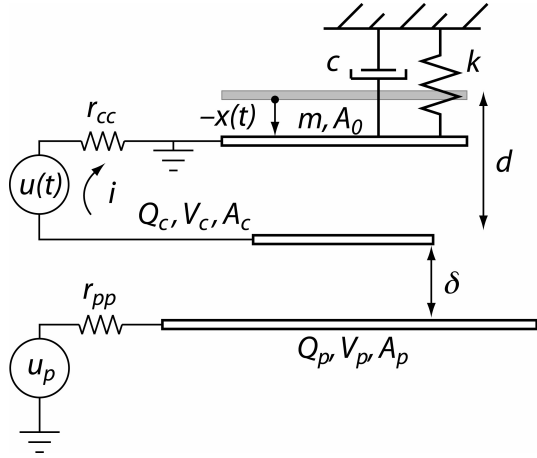


Figure 1. 1-DOF MODEL OF A ELECTROSTATIC MICROACTUATOR. THE TOP PLATE OF THE MEMS IS FREE TO MOVE AND THE TWO BOTTOM PLATES ARE HELD FIXED. THE MIDDLE PLATE IS THE CONTROL ELECTRODE AND THE BOTTOM PLATE IS THE PARASITIC ELECTRODE. THIS PARTICULAR CONFIGURATION IS AN EXAMPLE OF CASE II. THE AREA OF THE BOTTOM PLATE MAY BE REDUCED TO THAT OF THE TOP PLATE WITHOUT AFFECTING THE SIMPLE CAPACITANCE MODELS USED FOR CONTROL DESIGN. THE PARASITIC BIAS VOLTAGE u_p IS ASSUMED TO BE ZERO IN THE CONTROLLER DESIGN AND ANALYSIS.

device is surface micromachined on an insulating silicon dioxide or silicon nitride layer, which is in turn deposited on a (relatively conductive) silicon wafer. In such cases large parasitic capacitances may exist between the device and the underlying silicon, especially if the insulating layer is thin. In what follows, the parasitic bias voltage u_p shown in Fig. 1 is assumed to be zero.

For the purpose of control design the capacitive coupling and electrostatic forces are derived using a simple infinite parallel plate model that neglects fringing. Thus the mutual capacitance between any two surfaces will be $C_{ij} = \epsilon A_{ij}/l_{ij}$, where l_{ij} is the distance between the surfaces and A_{ij} is the area of the overlap between the surfaces *with no intervening conductor*. If the parasitic effects are due to interactions with a conductive substrate, this model allows us to consider only that portion of the substrate directly beneath the device. ϵ is the permittivity of the material in the gap between the plates, sometimes written as a dielectric constant times the permittivity of free space. In what follows, ϵ is simply a constant.

Even using the simplified 1-DOF model of Fig. 1 several distinct electrode configurations are possible. The following observation facilitates the analysis: Under the simplified capacitance calculation, the largest electrode area may, without loss of generality, be reduced to that of the next largest, resulting in three possible situations, in which either the parasitic electrode is the smallest, the control electrode is the smallest, or the mov-

able electrode is the smallest. The first and third are qualitatively very similar and the third may be easily treated by analogy to the first. Therefore, to avoid unnecessarily complex notation, we will consider only the first and second configurations, which we subsequently refer to as Case I and Case II. We define the parameter $\rho = A_p/A_c$. For Case I, $\rho \leq 1$ and for Case II $\rho \geq 1$. Note that in Case I the movable electrode is completely screened from the parasitic electrode by the control electrode. In Case II the movable electrode is directly affected by the parasitics.

The configuration space of the movable electrode is $G = \mathcal{R}$. Let $\{e_1\}$ be a coordinate frame for \mathcal{R} , with e_1 fixed at the center of mass of the moving electrode in zero voltage equilibrium and pointing away from the fixed control electrode, and with x denoting the displacement of the movable electrode along e_1 . Then application of the modeling procedure presented in [2, 8], gives the following equations of motion:

$$\dot{Q}_c = -\frac{1}{r_{cc}}V_c + \frac{1}{r_{cc}}u_c, \quad (1)$$

$$= -\frac{1}{r_{cc}}C^{cp}(x)(\alpha^{cc}(x)Q_c + Q_p) + \frac{1}{r_{cc}}u_c, \quad (2)$$

$$\dot{Q}_p = -\frac{1}{r_{pp}}C^{cp}(x)(Q_c + \alpha^{pp}(x)Q_p), \quad (3)$$

$$\dot{x} = v, \quad (4)$$

$$\dot{v} = -2\zeta\omega v - \omega^2 x - f^e(x, Q_c, Q_p), \quad (5)$$

where $f^e(x, Q_c, Q_p)$ is of the form

$$f^e(x, Q_c, Q_p) = \frac{1}{2m\epsilon A_0} (f_{11}^e(x)Q_c^2 + 2Q_cQ_p + Q_p^2),$$

Charge and voltage are related by

$$\begin{bmatrix} V_c \\ V_p \end{bmatrix} = C^{cp} \begin{bmatrix} \alpha^{cc} & 1 \\ 1 & \alpha^{pp} \end{bmatrix} \begin{bmatrix} Q_c \\ Q_p \end{bmatrix} \quad (6)$$

where $C^{cp}(x) = (x+d)/\epsilon A_0$, and the voltage V_c on the drive electrode is assumed to be measured. The two electrode configuration cases differ only in α^{cc} , α^{pp} , and f_{11}^e . The situation is summarized in Table 1.

VOLTAGE AND CHARGE PULL-IN

It is instructive to review the system without parasitics, and recall how the choice of charge as the controlled output eliminates the voltage pull-in bifurcation. In this case (3) is omitted, the Q_p terms do not appear in (2), or (5), and $\alpha^{cc}(x) = f_{11}^e(x) = 1$. The simplified capacitance models imply that, without loss of generality, A_c and A_0 may be assumed equal to the smaller of

Case	I	II
Smallest Area	A_p	A_c
Other Areas	$A_c = A_0$	$A_p = A_0$
f_{11}	1	$1 + \frac{\delta^2(\rho-1)}{(x+d+\delta)^2}$
α^{cc}	1	$1 + \frac{\delta(\rho-1)}{x+d+\delta}$
α^{pp}	$1 + \frac{\delta}{\rho(x+d)}$	$1 + \frac{\delta}{x+d}$

Table 1. EXPRESSIONS APPEARING IN (1)–(5) FOR THE TWO ELECTRODE GEOMETRY CASES. $\rho \equiv A_p/A_c$.

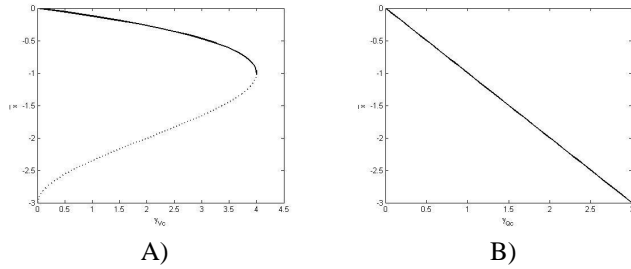


Figure 2. BIFURCATION DIAGRAM FOR THE ZERO DYNAMICS OF A 1-DOF MEMS MODEL WITHOUT PARASITICS. SOLID LINES DENOTE STABLE EQUILIBRIA, DASHED LINES DENOTE UNSTABLE EQUILIBRIA. A) VOLTAGE CONTROL. B) CHARGE CONTROL.

the two, here arbitrarily denoted A_c . For the voltage control case the output is chosen as $y = V_c(x, Q_c) - \bar{V}_c = (d+x)Q_c/\epsilon A_0 - \bar{V}_c$. Thus, at equilibrium, $y \equiv 0$ implies $\bar{Q}_c = \epsilon A_0 \bar{V}_c / (d+\bar{x})$. The relative degree of the system is one, and the zero dynamics are the dynamics of the mechanical subsystem. Any equilibrium of the zero dynamics must satisfy $\bar{v} = 0$ and

$$-(\bar{x}+d)^2 \bar{x} = \frac{\epsilon A_0 \bar{V}_c^2}{2m\omega^2} \equiv \gamma_{V_c}. \quad (7)$$

Figure 2(a) plots the roots of 7 that fall in the physical region $-d \leq \bar{x} \leq 0$ versus a bifurcation parameter, γ_{V_c} , which is simply the value of the right-hand side of (7). A particular value of γ_{V_c} corresponds to two, one, or no equilibrium points. When there are two equilibria the one closer to the origin is stable, the other is unstable, as shown in the figure. Voltage pull-in corresponds to the saddle-node bifurcation that occurs at $\bar{x} = -d/3$, where there is a single equilibrium in the feasible region. For charge control the output is chosen as $y \equiv Q_c - \bar{Q}_c$. The zero dynamics are again the dynamics of the mechanical subsystem, now with

equilibria satisfying $\bar{v} = 0$ and

$$-\bar{x} = \frac{\bar{Q}_c^2}{2\epsilon A_0 m \omega^2} \equiv \gamma_{Q_c}. \quad (8)$$

Figure 2(b) plots the roots of (8) that fall within the feasible region versus the right-hand side, γ_{Q_c} . Now a particular value of γ_{Q_c} corresponds either to a unique stable equilibrium point, or to no equilibrium point. The voltage pull-in bifurcation is eliminated. This observation, as well as being implicitly exploited in several previous studies such as [10, 14], was the basis for the 1-DOF passivity controller in [7], and the motivation for the general method presented in [8].

Case	I	II
\bar{Q}_p	$-\frac{\bar{Q}_c \rho (\bar{x}+d)}{\rho \bar{x} + \rho d + \delta}$	$-\frac{\bar{Q}_c (\bar{x}+d)}{\bar{x}+d+\delta}$
$f^e(\bar{x}, \bar{Q}_c, \bar{Q}_p)$	$\frac{\delta^2 \bar{Q}_c^2}{2m\epsilon A_0 (\rho \bar{x} + \rho d + \delta)^2}$	$\frac{\rho \delta^2 \bar{Q}_c^2}{2m\epsilon A_0 (\bar{x}+d+\delta)^2}$

Table 2. EQUILIBRIUM CONDITIONS WITH OUTPUT Q_c .

With the parasitic surface included in the model, it can be verified that for both Cases I and II voltage control gives zero dynamics equilibrium conditions identical to (7). Therefore voltage pull-in bifurcation occurs as before. Charge control, however, is fundamentally altered by the presence of the parasitics. The equation governing the equilibrium position of the electrode becomes for Case I

$$-(\bar{x}+d + \frac{\delta}{\rho})^2 \bar{x} = \frac{\delta^2 \bar{Q}_c^2}{2\epsilon A_0 m \omega^2 \rho^2}. \quad (9)$$

Comparing (9) to (7) we see that there will be a saddle-node bifurcation, referred to “charge pull-in.” It occurs at $\bar{x} = (d/3) + (\delta/3\rho)$ which is greater than $d/3$. If $\frac{\rho d}{\delta} \leq 1/2$ then charge pull-in does not occur in the physically feasible region. For Case II the equilibrium equations are

$$-(\bar{x}+d+\delta)^2 \bar{x} = \frac{\rho \delta^2 \bar{Q}_c^2}{2\epsilon A_0 m \omega^2}. \quad (10)$$

Once again charge pull-in occurs, this time at a critical displacement of $(d/3) + (\delta/3)$, again greater than $d/3$. Therefore, as was first noted in [5], charge control confers a greater operating range than voltage control, even in the presence of parasitics. However, as δ becomes small or ρ becomes large, any advantage becomes

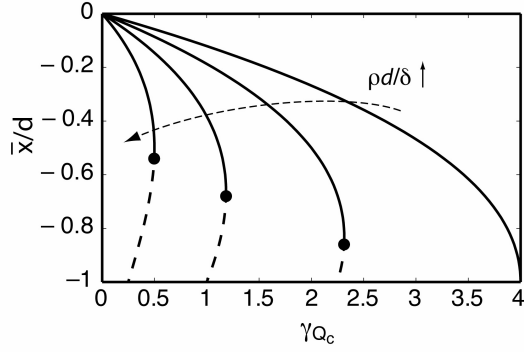


Figure 3. EQUILIBRIUM CURVES FOR THE ZERO DYNAMICS OF A 1-DOF MEMS MODEL UNDER CHARGE CONTROL WITH PARASITICS AS PARAMETER $\rho d/\delta$ VARIES.

vanishingly slight. Figure 3 shows this behavior graphically as the parameter $\rho d/\delta$ varies.

From a passivity point of view, in the absence of parasitics the choice of charge as the output instead of voltage eliminates voltage pull-in. However parasitics induce the related phenomenon of charge pull-in. Then it is natural to ask whether there is another system output, for which charge pull-in does not occur. The next section demonstrates that there is.

PASSIVITY-BASED CONTROL WITH PARASITICS

Case	I	II
\bar{Q}_p	$-\frac{\rho(\bar{x}+d)}{\delta}\bar{Q}_e$	$-\frac{\bar{x}+d}{\delta}\bar{Q}_e$
$f^e(\bar{x}, \bar{Q}_e, \bar{Q}_p)$	$\frac{\bar{Q}_e^2}{2m\epsilon A_0}$	$\frac{\rho\bar{Q}_e^2}{2m\epsilon A_0}$
\bar{x}	$-\frac{\bar{Q}_e^2}{2m\epsilon A_0\omega^2}$	$-\frac{\rho\bar{Q}_e^2}{2m\epsilon A_0\omega^2}$

Table 3. EQUILIBRIUM CONDITIONS WITH TOTAL CHARGE Q_e AS OUTPUT.

In the absence of parasitics, $f^e(x, Q_c)$ in (5) is $Q_c^2/2m\epsilon A_0$. With parasitics, for Case I, $f_{11}^e = 1$, and so $f^e(x, Q_c, Q_p) = (Q_c + Q_p)^2/2m\epsilon A_0$. This suggests that choosing as system output the *total charge* $Q_e \equiv Q_c + Q_p$ will eliminate the charge pull-in bifurcation. This result is immediate for Case I. For Case II, the substitution $Q_c = Q_e - Q_p$ yields a less clear-cut expression:

$$f^e(x, Q_e, Q_p) = \frac{Q_e^2}{2m\epsilon A_0} + \frac{\delta^2(\rho - 1)}{(x + d + \delta)^2} \frac{(Q_e - Q_p)^2}{2m\epsilon A_0} \quad (11)$$

However solving for \bar{Q}_p in terms of \bar{x} gives the same equilibrium equation as for Case I. These results are summarized in Table 3. In both cases the system with total charge as output has relative degree one and a unique equilibrium point. The elimination of charge pull-in suggests that any feasible equilibrium may be made globally asymptotically stable, but, as will be seen, this is not true. Three problems arise, all associated only with Case II. The first is that the arguments for global stability of the equilibrium no longer hold, and in fact simulations show that the region of attraction is finite. The second is that while the charge pull-in saddle-node bifurcation has been eliminated, the unique equilibrium may lose stability via a Hopf bifurcation. The third is that in this case Q_e feedback is not implementable from the assumed measurements x , V_c , and Q_c . An approximation must be used, which further reduces the region of attraction.

We transform the system (1)–(5) from (Q_c, Q_p, x, v) to (Q_e, Q_p, x, v) coordinates, and proceed as in [7] by applying the input-output linearizing control

$$u_c = r_{cc} \left(\left(\frac{1}{r_{cc}} + \frac{\alpha^{pp}(x)}{r_{pp}} \right) V_c + \frac{C^{cp}(x)(1 - \alpha^{cc}(x)\alpha^{pp}(x))}{r_{pp}} Q_c + v \right) \quad (12)$$

to obtain the following system:

$$\dot{Q}_e = v, \quad (13)$$

$$\dot{x} = v, \quad (14)$$

$$\dot{v} = -2\zeta\omega v - \omega^2 x - f^e(x, Q_e, Q_p), \quad (15)$$

$$\dot{Q}_p = \frac{C^{cp}(x)}{r_{pp}} ((\alpha^{pp}(x) - 1)Q_p + Q_e), \quad (16)$$

where

$$f^e(x, Q_e, Q_p) = \frac{1}{2m\epsilon A_0} (Q_e^2 + (f_{11}^e(x) - 1)(Q_e - Q_p)^2)$$

A stabilizing energy-shaping controller may be designed for Case I following [8],:

$$v = -k(Q_e - \bar{Q}_e) \quad (17)$$

where $k > 0$. The choice of Q_e as output ensures a unique equilibrium point for every $-d \leq \bar{x} \leq 0$. For Case I (13)–(15) reduce exactly to the equations without parasitics, with Q_e replacing Q_c . Thus repeating the proof in [7] for this case shows that the controller (17) globally asymptotically stabilizes any desired feasible equilibrium. Implementation requires Q_e . For Case I we find

from (6) the following expression for Q_e in terms of V_c and x :

$$Q_e = \frac{\epsilon A_c}{x+d} V_c. \quad (18)$$

Therefore, assuming availability of x , V_c , and Q_e , a static output feedback controller may be implemented for Case I as

$$v = -k \left(\frac{\epsilon A_c}{x+d} V_c - \bar{Q}_e \right). \quad (19)$$

Furthermore, as long as the various modeling assumptions are valid, the performance of Case I will be identical to the nominal case investigated in [7].

In Case II the expression for Q_e also contains a term involving the parasitic voltage:

$$Q_e = \frac{\epsilon A_c}{x+d} V_c + \frac{\epsilon A_c (\rho - 1)}{x+d+\delta} V_p. \quad (20)$$

Thus it is infeasible to implement the Q_e controller with available measurements for Case II. We propose to neglect the V_p term in (20), and to approximate Q_e in Case II by (18), that is, $\hat{Q}_e = \epsilon A_c V_c / (x+d)$. So we obtain for Case II the same controller (19) as for Case I. Due to the assumption of zero parasitic bias voltage in the system model (1)–(5), $\bar{V}_p = 0$. Therefore the use of (18) in steady state gives the correct value of \bar{Q}_e , even for Case II. Then the results of Table 3 are still valid, and charge pull-in bifurcation will not occur. Next we note that for ρ close to unity the V_p term in (20) is small, and so it is reasonable to expect that in such situations the unique equilibrium will be stable and the region of attraction large.

In summary, we have shown in this section that the output feedback controller (19) eliminates charge pull-in for both Case I and Case II. For Case I we also have global asymptotic stability of the resulting unique equilibrium point. For Case II we have no stability guarantee, but for ρ close to one we expect robust stability. Recall that under the simplified capacitance models used, the area of the parasitic surface can be taken in Case II to be equal to the area of the movable electrode. Therefore ρ may be estimated as the ratio of the area of the movable electrode to the area of the drive electrode. In actual MEMS devices this is often close to one, and rarely greater than ten. The following section uses Matlab simulation to examine the stability of the equilibrium as ρ increases.

SIMULATION RESULTS

This section presents three sets of simulation results focusing on Case II. First we show the existence of a subcritical Hopf

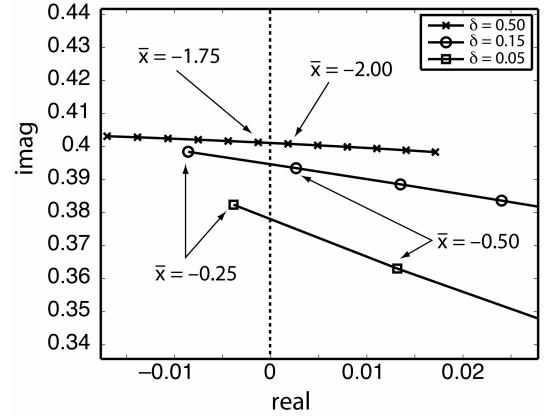


Figure 4. COMPLEX CONJUGATE ROOTS CROSSES INTO THE RIGHT HALF-PLANE, SIGNALING A HOPF BIFURCATION, AS \bar{x} INCREASES FOR VARIOUS VALUES OF δ AND WITH $\rho = 1.5$

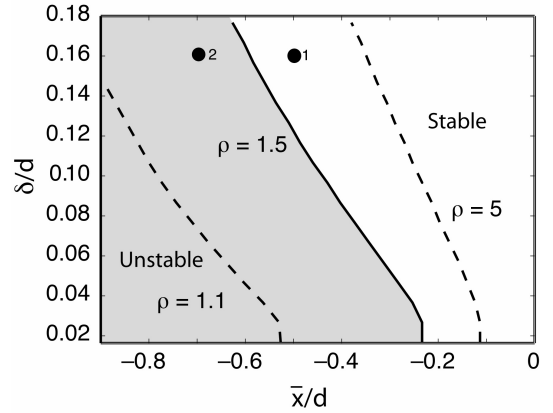


Figure 5. STABILITY BOUNDARIES IN THE NORMALIZED \bar{x} - δ PARAMETER SPACE FOR $\rho = 1.1, 1.5, \text{ AND } 5$. THE DAMPING RATIO IS SET TO $\zeta = 0.05$. AS ρ INCREASES AND/OR δ DECREASES THE BIFURCATION VALUE OF \bar{x} INCREASES, INDICATING LOSS OF STABILITY OF EQUILIBRIUM POINTS HIGHER IN THE GAP.

bifurcation associated with the zero dynamics using total charge feedback as output. These results use Q_e set exactly to \bar{Q}_e , and therefore the bifurcation occurs even when the exact expression for total charge is used. Next we present Matlab simulations that validate the stabilizing properties of total charge feedback control by showing successful stabilization of a case for which charge pull-in makes Q_c control unstable. Finally we show more detailed simulation results using the ANSYS finite-element package, which show the effect of neglecting fringing in the controller .

Figure 4 shows the locus of one of a conjugate pair of complex roots of the linearized zero dynamics of (13)–(15) as \bar{x} varies

for fixed ρ and three different values of δ . A pole crosses into the right half-plane, signaling a Hopf bifurcation, for each value of δ considered. Figure 5 shows stable and unstable regions in the δ - \bar{x} parameter space for various values of ρ . It is important to know whether the Hopf bifurcation is subcritical or supercritical. In the former, an unstable limit cycle coexists around the stable equilibrium point, shrinking in amplitude as the bifurcation parameter nears its critical value, and collapsing onto the equilibrium at the bifurcation point. In the latter, a stable limit cycle coexists around the unstable equilibrium, again shrinking in amplitude as the bifurcation parameter nears its critical value, and collapsing on it at the bifurcation point [18]. Poincare sections along the x -axis were generated using Matlab simulation of trajectories in the x - v phase space, with Q_e and Q_p held at their equilibrium values. Figure 6 shows the result for parameters corresponding to Point 1 from Fig. 5. An unstable limit cycle can be clearly seen. A similar numerical analysis at Point 2 is not shown, but displays no sign of a limit cycle. Since an unstable limit cycle coexists around the stable equilibrium point, we conclude that the bifurcation is subcritical.

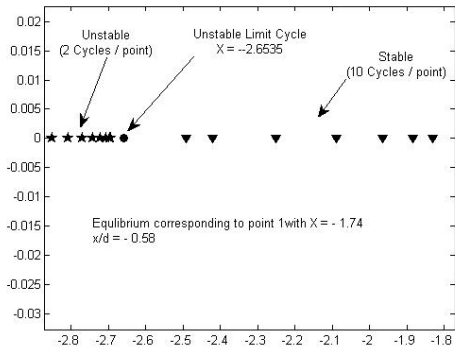


Figure 6. A POINCARÉ SECTION FOR POINT 1 FROM FIG. 5 SHOWING AN UNSTABLE LIMIT CYCLE AROUND THE STABLE EQUILIBRIUM POINT. Q_e and Q_p ARE SET TO THEIR EQUILIBRIUM VALUES.

Figure 7 shows how Q_c control results in charge pull-in in the presence of parasitics, while Q_e control is stabilizing. Figure 8 shows the effect of neglecting fringing in the controller. The simplified parallel plate capacitance models are used twice. First, they are used to obtain the \bar{Q}_e that will give a desired position \bar{x} . Next, they are implicit in the linearizing feedback (12). The figure applies the controller in an ANSYS simulation, in which the electrode capacitances are computed using finite-element analysis. This analysis incorporates fringing, which is neglected in the parallel plate approach. The results show that an error of about 6% is associated with use of the approximate capacitance values

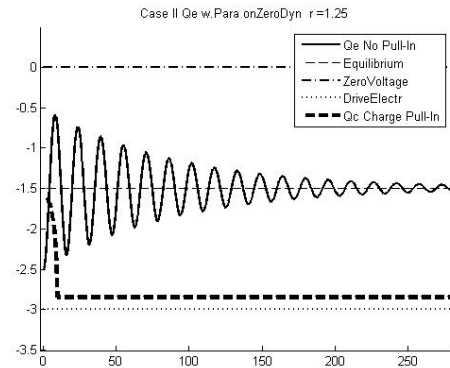


Figure 7. A COMPARISON OF Q_c CONTROL AND Q_e CONTROL FOR A CASE II DEVICE WITH $\rho = 1.25$. THE Q_c CONTROLLER EXHIBITS CHARGE PULL-IN, WHILE THE Q_e CONTROLLER IS STABILIZING.

in the linearizing feedback, while an error of about 4% is associated with the imperfect calculation of \bar{Q}_e . Together these give an error of over 10%. Remarkably this is the case even though the approximate parallel plate capacitance values themselves are very close to the computed ANSYS values, as seen in Fig. 9. We conclude by noting that the more accurate finite-element values could in principle be incorporated into the actual controller to provide improved performance.

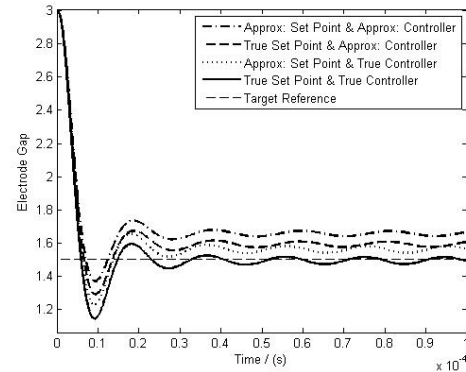


Figure 8. ANSYS SIMULATION USING PARALLEL PLATE AND COMPUTED CAPACITANCE MODELS.

CONCLUSION

This paper presents a 1-DOF model including a capacitively coupled parasitic electrode, specialized from a general modeling and controls framework for electrostatically actuated MEMS.

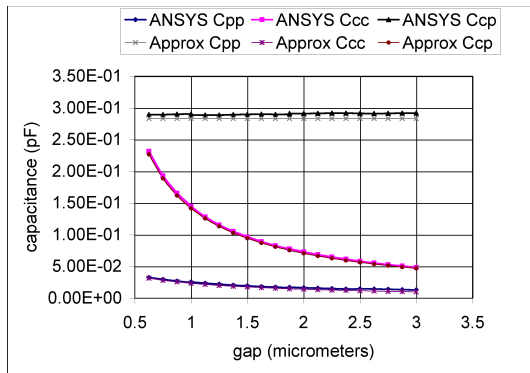


Figure 9. COMPARISON OF PARALLEL PLATE APPROXIMATIONS TO ANSYS COMPUTED CAPACITANCE VALUES.

Previous work by the authors presented static and dynamic output feedback controllers that, in the absence of parasitics, globally asymptotically stabilize any equilibrium electrode configuration, thereby eliminating voltage pull-in and allowing the movable electrode an extended travel range. These controllers were based on the observation that the bifurcation that occurs in the zero dynamics when drive electrode voltage is chosen as the system output does not occur when drive electrode charge is chosen instead. However a sufficiently large parasitic capacitance will destroy this property, and a saddle-node bifurcation will again occur. This phenomenon, known in the literature as *charge pull-in*, limits the operational range of travel of the movable electrode, though less severely than voltage pull-in. For the 1-DOF model considered, we show that the use of *total charge* as the system output eliminates the charge pull-in bifurcation. Two qualitatively different electrode geometries must be considered. In the first, we recover the global asymptotic stability result obtained without parasitics. In the second, depending on the size of the parasitic capacitance, the region of attraction of the unique closed-loop equilibrium point is finite, and in fact it may lose stability through a Hopf bifurcation. Furthermore, in the second geometry it is not possible to implement total charge feedback with feasible measurements. However an output feedback controller neglecting the unmeasurable quantities still eliminates the pull-in.

ACKNOWLEDGMENTS

The support of the National Science Foundation under grants ECS-0218345 and ECS-0220314 is gratefully acknowledged.

REFERENCES

[1] R. C. Anderson, B. Kawade, D. H. S. Maithripala, K. Ragan, J. M. Berg, R. O. Gale, "Integrated charge sensors

for feedback control of electrostatic MEMS," *Proceedings of the SPIE conference on Smart Structures and Materials 2005: Sensors and Smart Structures Technologies for Civil, Mechanical, and Aerospace Systems*, San Diego, 6-10 March 2005.

- [2] Jordan M. Berg, D. H. S. Maithripala, B. D. Kawade, and W. P. Dayawansa, "Integrated Modeling and Control of Electrostatic MEMS, Part I: Modeling," *Proceedings of the IEEE International Conference on Information and Automation*, December 15–18, 2005, Colombo, Sri Lanka.
- [3] C. I. Byrnes, A. Isidori and J. C. Willems, "Passivity, Feedback Equivalence, and the Global Stabilization of Minimum Phase Nonlinear Systems," *IEEE Transactions on Automatic Control*, (36) No. 11, pp 1228 – 1240, Nov 1991.
- [4] E. K. Chan, R. W. Dutton, "Electrostatic micromechanical actuator with extended range of travel," *Journal of Microelectromechanical Systems*, Vol. 9, No. 3, pp. 321–328, 2000.
- [5] D. Elata, O. Bochobza-Degni and Y. Nemirovsky, "Analytical Approach and Numerical Alpha-Line Method for Pull-In Hyper-Surface Extraction of Electrostatic Actuators with Multiple Uncoupled Voltage Sources," *Journal of Microelectromechanical Systems*, Vol. 12, No. 5, pp. 681–691, Oct 2003.
- [6] B. D. Kawade, D. H. S. Maithripala, and J. M. Berg, "Efficient Multi-Physics Transient Analysis Incorporating Feedback-Dependent Boundary Conditions," *Proceedings of the 2006 ANSYS Users Conference*.
- [7] D. H. S. Maithripala, J. M. Berg and W. P. Dayawansa, "Control of an Electrostatic MEMS Using Static and Dynamic Output Feedback," *ASME Journal of Dynamical Systems Measurement and Control*, Vol 127, pp. 443 – 450, 2005.
- [8] D. H. S. Maithripala, B. D. Kawade, J. M. Berg, and W. P. Dayawansa, "A General Modeling and Control Framework for Electrostatically-Actuated Mechanical Systems," *International Journal of Robust and Nonlinear Control, Special Issue on Control at the Nanoscale*, Vol. 15, pp. 839 – 857, published online 15 September 2005.
- [9] D. H. S. Maithripala, B. D. Kawade, J. M. Berg and W. P. Dayawansa, "Integrated Modeling and Control of Electrostatic MEMS, Part II: Control," *Proceedings of the IEEE International Conference on Information and Automation*, December 15–18, 2005, Colombo, Sri Lanka.
- [10] R. Nadal-Guardia, A. Dehe, R. Aigner and L. McAstaner, "Current drive methods to extend the range of travel of electrostatic microactuators beyond the voltage pull-in point," *Journal of Microelectromechanical Systems*, Vol. 11, No. 3, pp. 255–263, June 2002.
- [11] M. Napoli, W. Zhang, K. Turner and B. Bamieh, "Characterization of Electrostatically Coupled Microcantilevers," *Journal of Microelectromechanical Systems*, Vol. 14, No. 2,

pp. 295–304, April 2005.

- [12] Y. Nemirovsky and O. Bochobza-Degni, “A Methodology for the Pull-In Parameters of Electrostatic Actuators,” *Journal of Microelectromechanical Systems*, Vol. 10, No. 4, pp. 601–615, Dec 2001.
- [13] R. Ortega, A. J. van der Schaft, I. Mareels, and B. Maschke, “Putting Energy Back in Control,” *IEEE Control Systems Magazine*, April, pp. 18–33, 2001.
- [14] J. I. Seeger and B. E. Boser, “Charge Control of Parallel-Plate, Electrostatic Actuators and the Tip-In Instability,” *Journal of Microelectromechanical Systems*, Vol. 12, No. 5, pp. 656–671, October 2003.
- [15] G. Zhu, J. Levine, and L. Praly, “On the Differential Flatness and Control of Electrostatically Actuated MEMS,” *Proceedings of the ACC*, Portland, Oregon, 2005.
- [16] G. C. Zhu, J. Levine, L. Praly, and Y. A. Peter, “Flatness-based control of electrostatically actuated MEMS with application to adaptive optics: A simulation study,” *Journal of Microelectromechanical Systems*, Vol. 15, No. 5, pp. 1165–1174, 2006.
- [17] G. C. Zhu, J. Penet, and L. Saydy, “Modeling and Control of Electrostatically Actuated MEMS in the Presence of Parasitics and Parametric Uncertainties,” *Journal of Dynamic Systems, Measurement, and Control*, in press.
- [18] J. K. Hale and H. Kocak, *Dynamics and Bifurcation*, Springer-Verlag, NY, 1996.